Presented at the 2012 MPIF / APMI International Conference on Powder Metallurgy & Particulate Materials held in Nashville, USA in June 2012 and published in the Advances in Powder Metallurgy &Particular Materials - 2012 conference proceedings available from the Metal Powder Industries Federation.

Characterization of Mechanical Properties and Machining Performance of New Malleable Iron Powder Grades

M. Moravej, F. Chagnon and J. Campbell-Tremblay

Rio Tinto Metal Powders

ABSTRACT

A new iron powder grade has been developed to reach 7.5 g/cm³ after sintering. This grade is a malleable iron powder, MIP, in which the carbon is dispersed as graphite nodules in a ferritic matrix. This material achieves almost 100% densification through liquid phase sintering. The shape of the graphite particles can be controlled through proper admixed additions and adjustment of the sintering temperature profile. This material also shows good machining performance.

This paper describes the static and dynamic properties of pearlitic MIP materials. Also, the face turning performance was compared to that achieved with DI 80-55-06 and a powder forged FC-0205 material with 0.3% MnS.

INTRODUCTION

Supersolidus liquid phase sintering (SLPS) is a process requiring prealloyed powders that, when heated to an intermediate temperature between the solidus and liquidus, nucleate a liquid within each particle. The amount of liquid produced is a function of the alloy composition and sintering temperature. The individual particles partially melt and hence promote densification by capillary induced rearrangement[1-2]. The Fe-C system is well suited for SLPS. However, on cooling, because of the high concentration of carbon, a carbide structure can be produced, which negatively affects the mechanical properties[3]. These can be improved by a post-sintering heat treatment[4] but with an increase of the production costs due to this additional processing step. To solve this problem, a new malleable iron powder grade has been developed to produce PM parts with sintered densities of 7.5 g/cm³ through supersolidus liquid phase sintering (SLPS)[5-6]. This new powder grade is produced by water atomization of a Fe-2C-1Si melt, which

is afterward submitted to a malleabilization heat treatment to produce a powder exhibiting a ferritic matrix with graphite nodules evenly distributed in the core and surface of the iron particles, Figure 1. This Fe-C-Si system is well suited to SLPS because the carbon is fully prealloyed and makes the sintering possible at around 1160°C. With the proper sintering profile, a pearlitic structure with a mixture of round and flaky graphite particles can be achieved. However, even if the presence of flaky graphite particles is not detrimental to the static properties, it has a negative effect on fatigue strength when the "nb flakes/mm² >100 µm" exceeds four[5]. Also, because of the presence of free graphite, parts made with this new powder grade would exhibit good machining performances. Therefore the objective of this paper is to describe the work done to modify the shape of the graphite particles from a flaky to nodular shape and to compare the machining characteristics of the new materials to those of DI 80-55-06 and a powder forged FC-0205 material with 0.3% MnS.

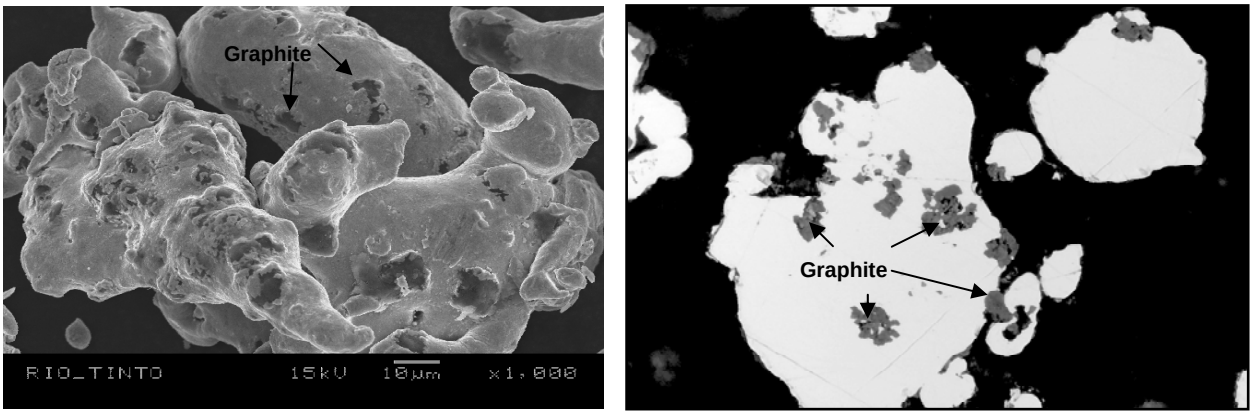

Figure 1. Particle shape and distribution of graphite nodules in MIP particles[5].

METALLURGICAL BACKGROUND OF MIP POWDERS

The base powder used in this study is a malleable iron powder, MIP, produced by water atomization of a Fe-2C-1Si melt. Table 1 shows the typical chemical and physical properties of this powder grade. When sintering at 1160°C, the carbon atoms are completely soluble in either the austenite or in the liquid. Therefore, on cooling, because there is no nucleation sites that remain within the grains, graphite precipitates preferentially at the grain boundaries with a flaky shape[5]. In order to retain free graphite in the core of MIP particles, the sintering temperature was decreased through the introduction of 0.2% P as admixed ferrophosphorus. Indeed, as shown in Figure 2, FactSage predicts that a liquid phase is present at 1120°C for a Fe-2C-1Si-0.2P system. Free graphite particles are retained at a sintering temperature of 1120°C. When the specimens are cooled from the sintering temperature, the carbon present in the liquid precipitates in both the residual porosity or the original graphite clusters in the ferrous matrix, and hence prevents the precipitation of graphite flakes. Table 2 describes the mix composition and the identification of both materials, called MIP-A and MIP-B.

Table 1. Chemical and physical properties of MIP.

C, %	O, %	Si, %	S, %	+60 mesh, %	-60/+100 mesh, %	-100/+325 Mesh, %	-325 mesh, %	Apparent density, g/cm³	Flow, s/50g
1.97	0.10	1.05	0.001	Trace	17	63	20	2.85	30

Table 2. Mix composition

	P, %	Lub, %
MIP-A	0	0.5
MIP-B	0.2	0.5

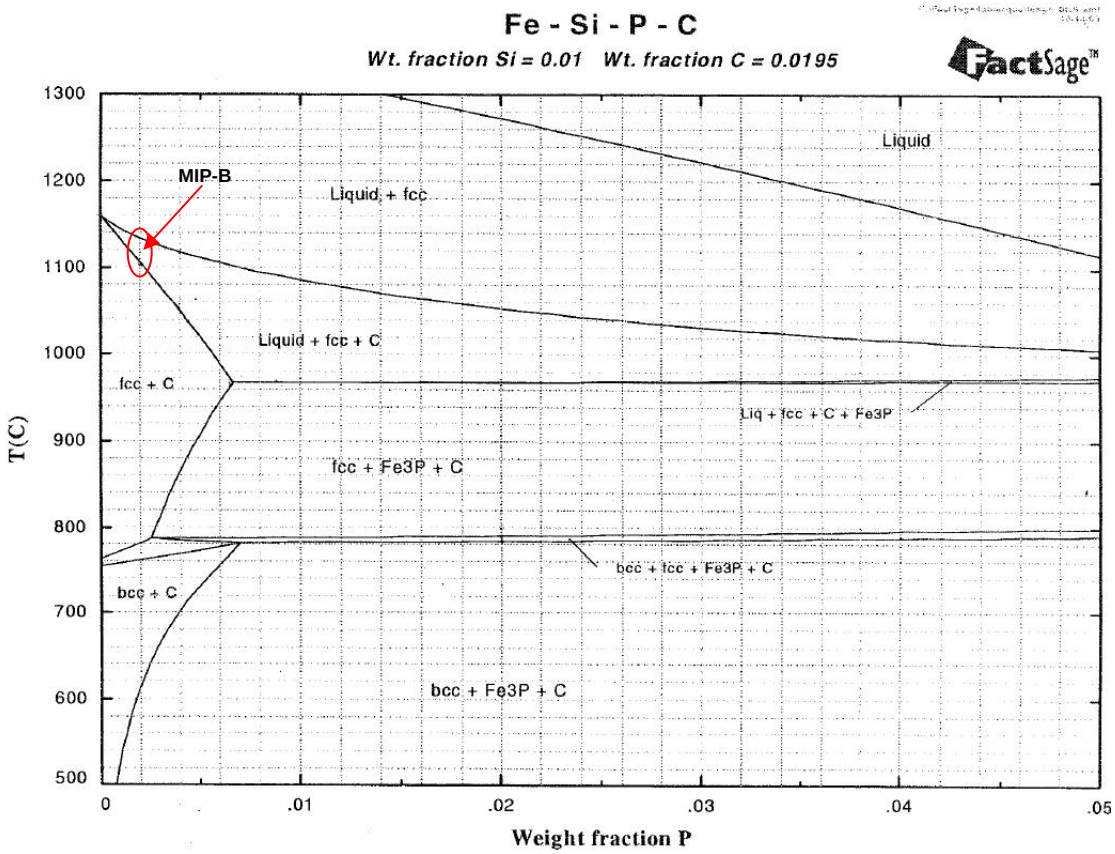

Figure 2. Equilibrium phase diagram for the Fe-C-Si-P system at 1120°C.

EXPERIMENTAL PROCEDURE

Rectangular bars (7.6 X 1.3 X 1.2 cm) were pressed at 6.6 g/cm³ to evaluate the effect of sintering temperature on dimensional change and sintered densities. These bars were machined in tensile, axial fatigue or un-notched impact energy specimens (MPIF Standards 10, 56 and 40, respectively). Axial fatigue resistance was evaluated at a load ratio of R = -1 using the staircase method with a runout limit of 10 million cycles. The bars pressed with MIP-A and MIP-B were sintered using the sintering parameters presented in Table 3. Figure 3 shows typical temperature profiles used to sinter both materials.

Table 3. Sintering parameters of MIP materials.

Material	MIP-A	MIP-B
Sintering atmosphere	90 % N_2 / 10 % H_2	90 % N_2 / 10 % H_2
Sintering temperature	1158 – 1166 °C	1118 – 1124 °C
Heating rate	1 °C/min (1140 °C - sintering temp.)	1 °C/min (1080 °C - sintering temp.)
Holding time	10 min	30 min
Cooling rate 1	1 °C/min (down to 1140 °C)	1 °C/min (down to 1100 °C)
Cooling rate 2	30 °C/min (1140 to 800 °C)	20 °C/min (1100 to 800 °C)
Cooling rate 3	1 °C /s (800 to 400 °C)	1 °C/s (800 to 400 °C)

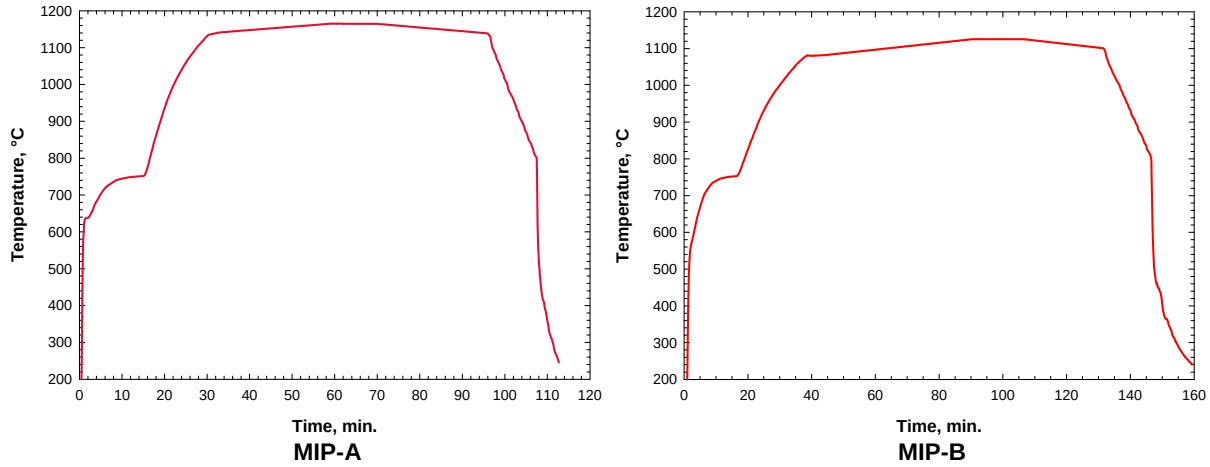

Figure 3. Temperature profiles used to sinter specimens pressed with MIP-A and MIP-B.

The microstructure was observed before and after etching by optical microscopy. The shape of the graphite particles was quantified by image analysis.

The machinability of MIP-A and MIP-B materials in face turning operation was evaluated and compared to that of DI 80-55-06 and a powder forged FC-0205 with 0.3% MnS. Face turning tests were performed using a Boehringer NG200 two spindle turning center. The work materials were pressed as rings having the following dimensions: 50.8 mm OD, 25.4 mm ID and 22.86 mm thickness. Two regimes of cutting operation were tested. One semi-roughing operation that involved two cutting speeds (183 and 274 m/min), one feed rate (0.254 mm/rev), and one depth of cut (1.52 mm). The second was a finishing operation which involved one cutting speed (137 m/min), one feed rate (0.102 mm/rev), and one depth of cut (1.02 mm).

Two types of tool holders (Figure 4) were used: DCKN and DCLN having 15° and –5° lead angles, respectively. The same insert shape and grade was used on both holders. The cutting forces were the variables monitored during turning tests. Forces were measured with a three-component 9121- type Kistler Dynamometer. Figure 5 shows the direction of the measured X, Y and Z cutting forces. A total of 24 tests were performed which are summarized in Table 4.

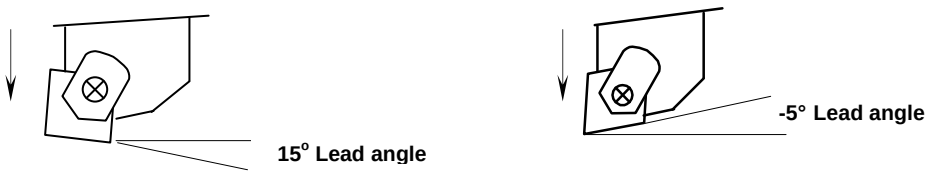

Figure 4. Tool holder geometry.

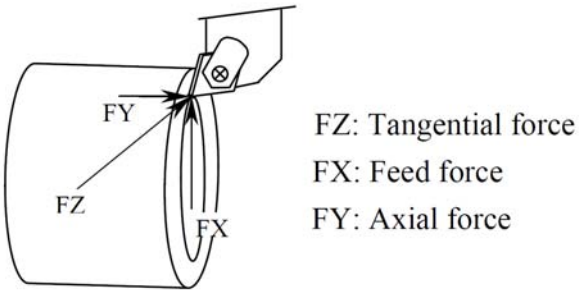

Figure 5. Direction of the cutting forces measured by the dynamometer at the insert/workpiece point of contact.

Table 4. Turning Test Parameters

Test	Material	Speed, m/min (ft/min)	Feed, mm/rev (in/rev)	DOC, mm (in)
Tests with tool holder/insert combination: DCLNL16 4D CNMG120408M5 - VP5515 (-5° lead angle)				
1	MIP-B	183 (600)	0.254 (0.01)	1.52 (0.06)
2	MIP-A	183 (600)	0.254 (0.01)	1.52 (0.06)
3	DI-80-55-06	183 (600)	0.254 (0.01)	1.52 (0.06)
4	FC-0205-0.3MnS	183 (600)	0.254 (0.01)	1.52 (0.06)
5	MIP-B	274 (900)	0.254 (0.01)	1.52 (0.06)
6	MIP-A	274 (900)	0.254 (0.01)	1.52 (0.06)
7	DI-80-55-06	274 (900)	0.254 (0.01)	1.52 (0.06)
8	FC-0205-0.3MnS	274 (900)	0.254 (0.01)	1.52 (0.06)
9	MIP-B	137 (450)	0.102 (0.004)	1.02 (0.04)
10	MIP-A	137 (450)	0.102 (0.004)	1.02 (0.04)
11	DI-80-55-06	137 (450)	0.102 (0.004)	1.02 (0.04)
12	FC-0205-0.3MnS	137 (450)	0.102 (0.004)	1.02 (0.04)
Tests with tool holder/insert combination: DCKNL16 4D CNMG120408M5 - VP5515 (15° lead angle)				
13	MIP-B	183 (600)	0.254 (0.01)	1.52 (0.06)
14	MIP-B	274 (900)	0.254 (0.01)	1.52 (0.06)
15	MIP-B	137 (450)	0.102 (0.004)	1.02 (0.04)
16	MIP-A	183 (600)	0.254 (0.01)	1.52 (0.06)
17	MIP-A	274 (900)	0.254 (0.01)	1.52 (0.06)
18	MIP-A	137 (450)	0.102 (0.004)	1.02 (0.04)
19	DI-80-55-06	183 (600)	0.254 (0.01)	1.52 (0.06)
20	DI-80-55-06	274 (900)	0.254 (0.01)	1.52 (0.06)
21	DI-80-55-06	137 (450)	0.102 (0.004)	1.02 (0.04)
22	FC-0205-0.3MnS	183 (600)	0.254 (0.01)	1.52 (0.06)
23	FC-0205-0.3MnS	274 (900)	0.254 (0.01)	1.52 (0.06)
24	FC-0205-0.3MnS	137 (450)	0.102 (0.004)	1.02 (0.04)

RESULTS AND DISCUSSION

Sintered density, dimensional change and microstructure

Figure 6 shows the densification curves of bars pressed from either MIP-A and MIP-B. Sintered densities in the range of 7.54-7.56 g/cm³ are reached in a temperature range of 1158 to 1166°C for specimens produced with MIP-A while for MIP-B, sintered densities ranging from 7.51 to 7.53 g/cm³ are reached between 1118 to 1124°C. Within these sintering windows, stable dimensional change values can be achieved. This is illustrated in Figure 7 where dimensional change values of -4.14 to -4.19% with MIP-A and -3.93 to -3.94% with MIP-B are observed in their respective temperature ranges. The slight difference observed between both materials is mainly related to the difference in final sintered densities of both materials, 7.55 and 7.52 g/cm³ for MIP-A and MIP-B, respectively.

Figure 8 shows typical unetched microstructures of specimens sintered at both ends of the sintering windows of the two materials. Specimens pressed with MIP-A show a combination of round and flake graphite particles mainly located at the grain boundaries. Graphite clusters precipitated during the solidification of the liquid phase and grew during the cooling stage as austenite-rejected carbon. For samples pressed with MIP-B, the graphite particles precipitated as small nodules not only at the grain boundaries but also within grains since graphite nuclei were not completely dissolved into austenite during the sintering stage.

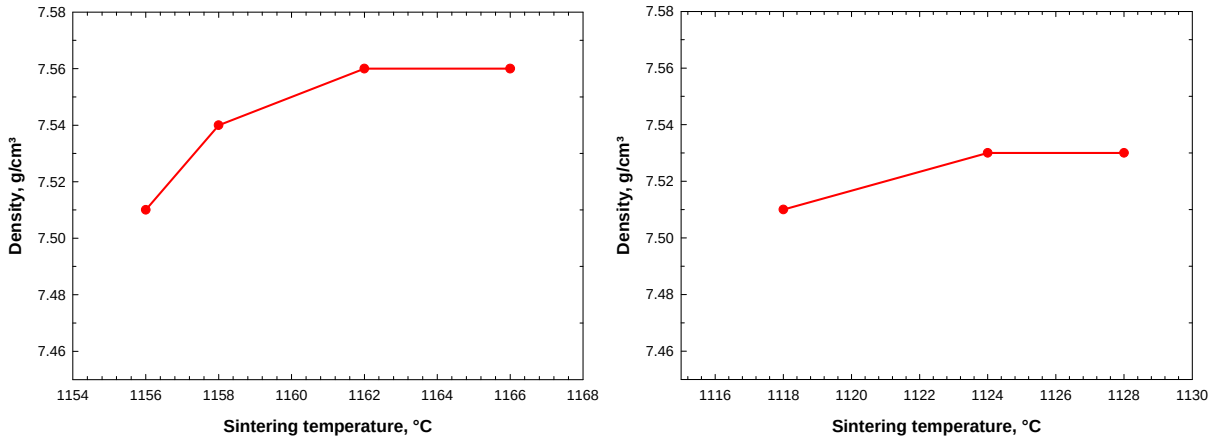

Figure 6. Densification curves of specimens pressed with MIP-A and MIP-B.

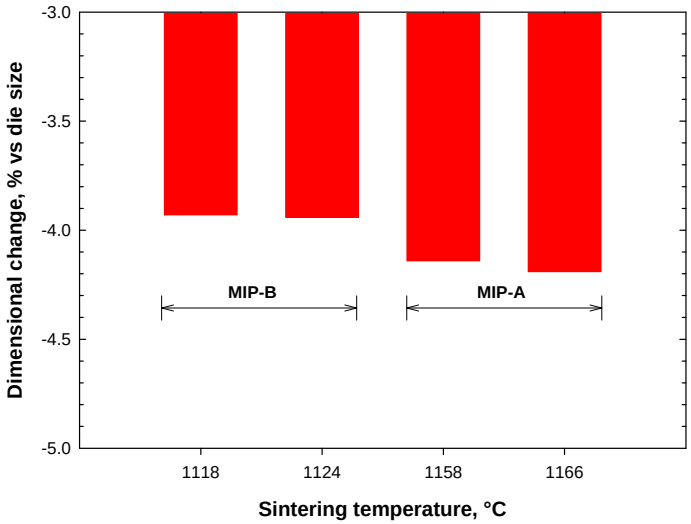

Figure 7. Dimensional change values measured within the sintering windows of MIP-B and MIP-A materials.

As illustrated in Figure 9, the number of graphite particles is almost three times higher in MIP-B than in MIP-A materials. Moreover, the number of graphite particles decreases as the sintering temperature increases. This is related to the increased volume fraction of liquid phase which contains a higher carbon concentration than solid austenite fraction. Since the potential sites for graphite precipitation were reduced while heating at high temperatures, the number of graphite particles was reduced during cooling. As the temperature increases, carbon diffuses from the graphite clusters towards the solid austenite and as the local carbon concentration in austenite reaches the concentration-temperature equilibrium, liquid appears in the powders. MIP-B exhibits a significantly higher proportion of graphite particles with a spherical shape as compared to MIP-A, 75 vs 50%, and the nodularity decreases more importantly with

MIP-A when the sintering temperature increases. Finally, MIP-A shows a larger "nb flakes/mm² >100µm" compared to MIP-B, 1.6 vs 0.2/mm². Also, in both materials, the formation of large flakes is promoted as the sintering temperature increases which emphasizes the importance to avoid oversintering.

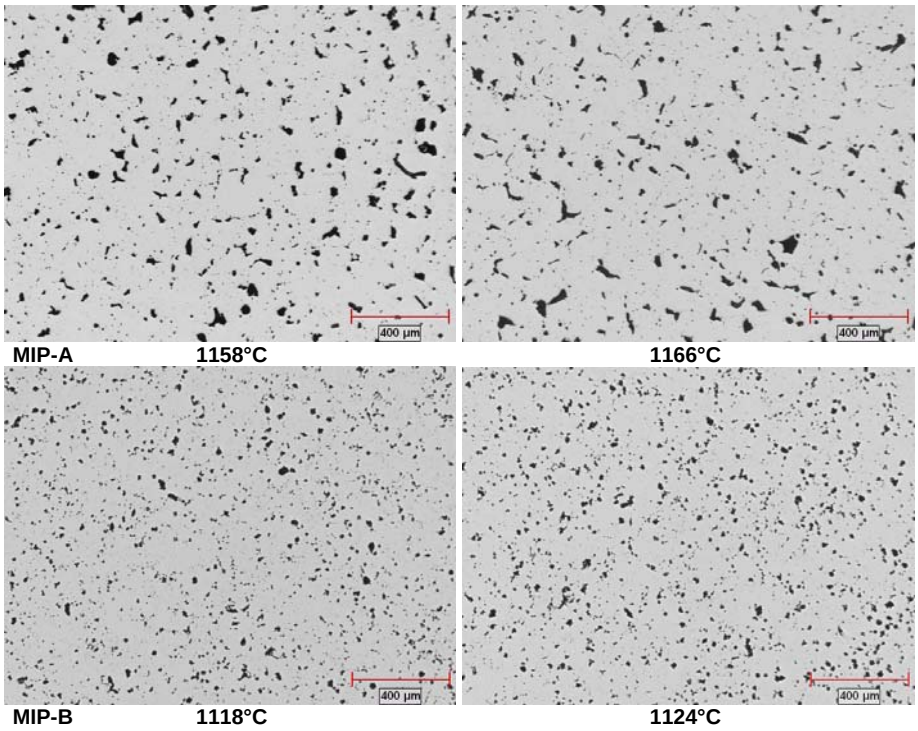

Figure 8. Unetched microstructure of specimens pressed from MIP-A sintered at 1158 and 1166°C and from MIP-B sintered at 1118 and 1124°C.

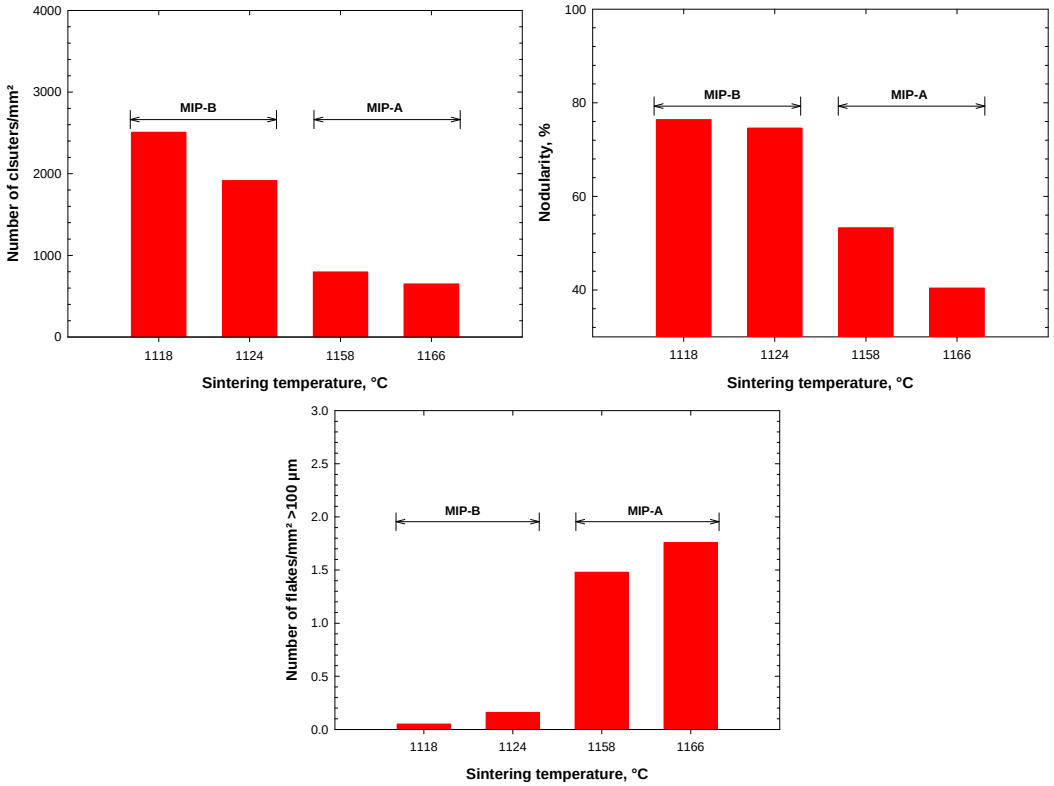

Figure 9. Density of "graphite particles/mm²", nodularity and "nb flakes/mm² >100 µm" in specimens sintered from MIP-B (1118 and 1124°C) and MIP-A (1158 and 1166°C).

Tensile properties, fatigue strength and impact strength

Table 5 summarizes the static and dynamic properties of specimens produced with MIP-A and MIP-B sintered at both ends of their sintering windows, i.e., 1158 and 1166°C for MIP-A and 1118 and 1124°C for MIP-B. For the impact strength, the sintering was carried out in the middle of the sintering window.

Figure 10 compares the tensile properties and hardness values measured with both materials. The first interesting observation is that when sintered in their respective sintering window, the tensile properties as well as hardness are not significantly affected by the sintering temperature. In the case of MIP-A, average tensile strength, yield strength, elongation and hardness values of respectively 788 MPa, 562 MPa, 1.8% and 29 HRC are reached compared to 876 MPa, 589 MPa, 2.5% and 28 HRC for MIP-B. As shown in Figure 11, these values are reached for a pearlitic microstructure. Indeed, both materials exhibit a structure of fine pearlite with the presence of a little fraction of ferrite surrounding the graphite particles.

Table 5. Sintered properties of specimens pressed from MIP-A sintered at either 1158 or 1166°C and MIP-B sintered at either 1118 or 1124°C

	MIP-A		MIP-B	
Temperature, °C	**1158**	**1166**	**1118**	**1124**
Sintered density, g/cm³	**7.53**	**7.56**	**7.51**	**7.53**
Tensile strength, MPa (ksi)	**780 (113)**	**795 (115)**	**884 (128)**	**868 (126)**
Yield strength, MPa (ksi)	**552 (80)**	**572 (83)**	**586 (85)**	**592 (86)**
Elongation, %	**1.82**	**1.78**	**2.6**	**2.5**

Hardness, HRC	**28**	**29**	**28**	**28**
Axial fatigue strength (R= -1; 50% surv.), MPa (ksi)	**241 (35)**	**279 (40)**	**312 (45)**	**333 (48)**
Temperature, °C	**1162**		**1121**	
Sintered density, g/cm³	**7.56**		**7.52**	
Impact energy, J	**33**		**22**	

Figure 12 compares the axial fatigue strength values of specimens pressed with MIP-A and MIP-B. The first important observation is that MIP-B material shows higher axial fatigue strength than MIP-A material, 323 vs. 260 MPa i.e. 20% higher. This can be related to the rounder shape of the graphite particles found in MIP-B. Indeed, in a previous work[5], it was shown that the presence of large concentration of long flakes was detrimental to fatigue resistance. These probably act as stress concentration sites for crack propagation. It is also worth noting that fatigue strength increases when the sintering temperature increases for both materials, from 241 MPa at 1158°C to 279 MPa at 1166°C for MIP-A, and from 312 MPa at 1118°C to 333 MPa at 1124°C for MIP-B. This can be related to the increase of the sintered density with the sintering temperature. This points out the importance of the sintered density on fatigue strength as also observed in a previous study[5].

Figure 13 compares the impact energy values of both materials sintered in the middle of their sintering window. Specimens pressed with MIP-A show an impact energy value of 33 joules compared to 22 joules for those pressed with MIP-B.

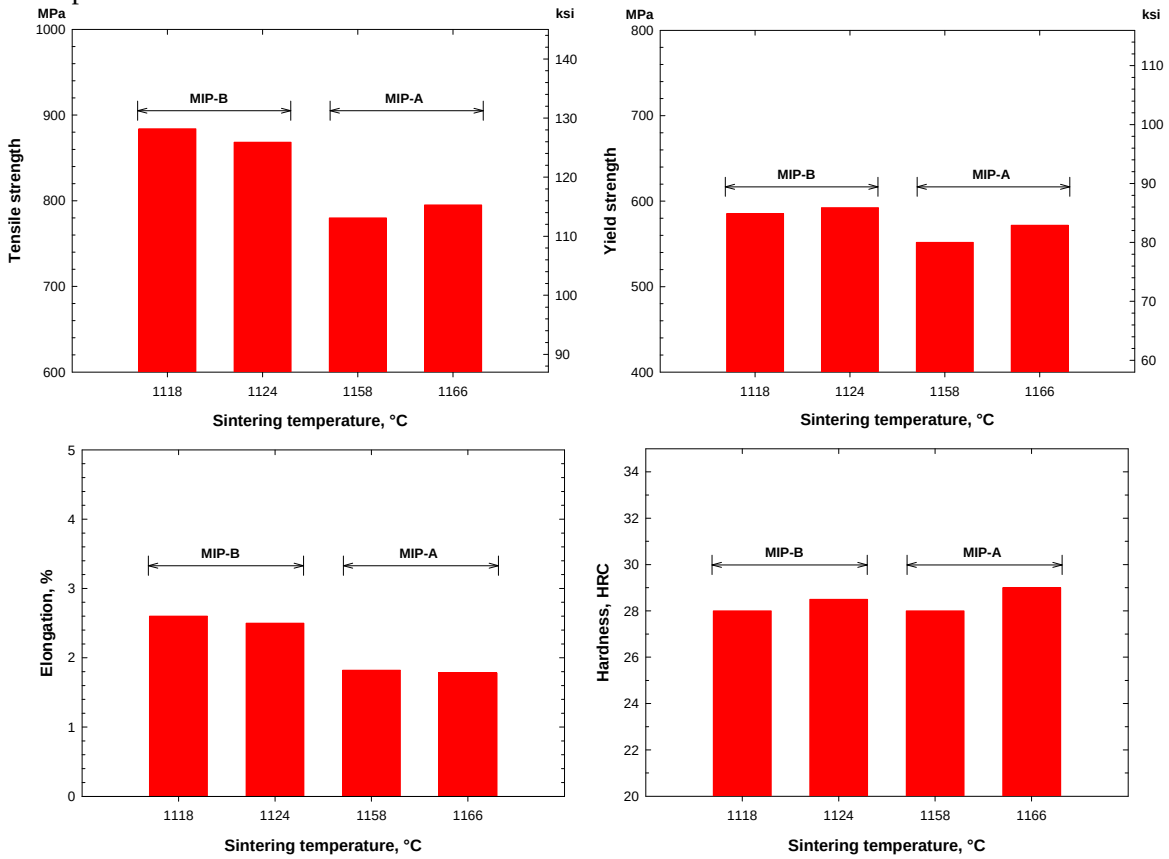

Figure 10. Tensile strength, yield strength, elongation and hardness of specimens pressed from MIP-B and MIP-A sintered at both ends of their sintering windows.

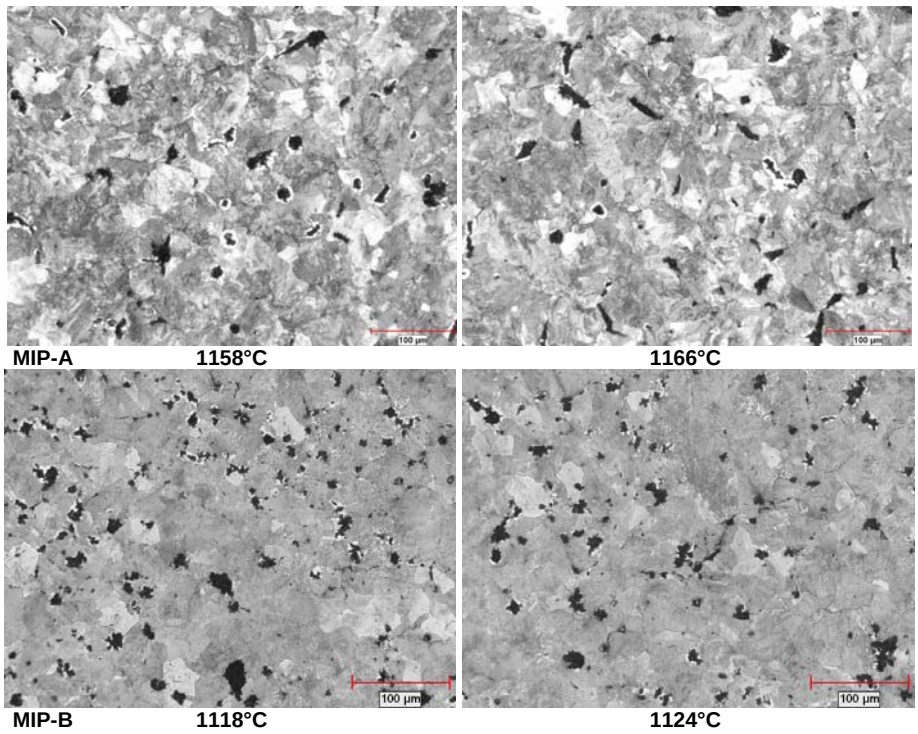

Figure 11. Etched microstructures of specimens pressed from MIP-A and MIP-B sintered at both ends of their sintering windows (Nital etching; 200X).

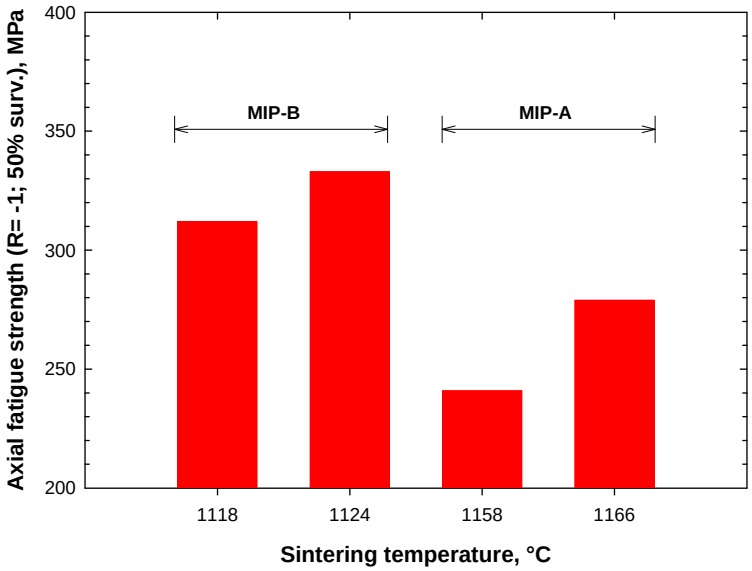

Figure 12. Axial fatigue strength of specimens pressed from MIP-B and MIP-A sintered at both ends of their sintering windows (R= -1; 50% survival).

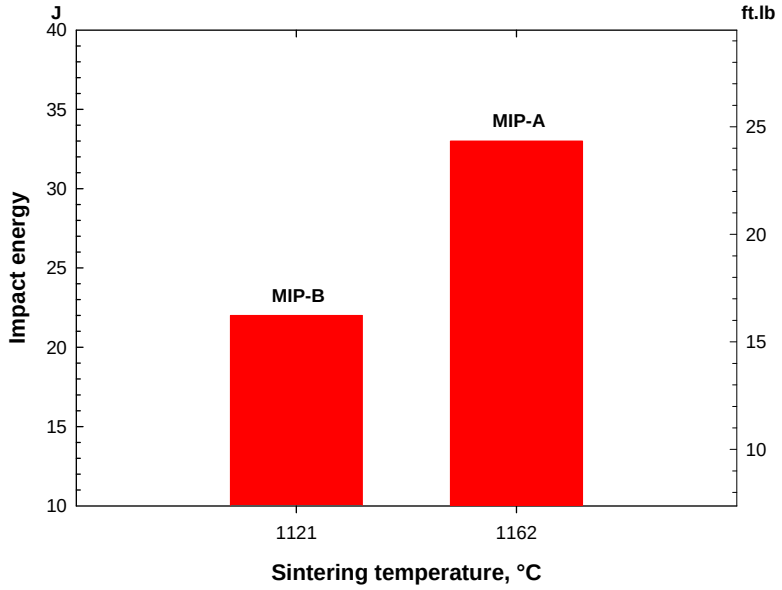

Figure 13. Impact energy measured with specimens pressed with MIP-B sintered at 1121°C and MIP-A sintered at 1162°C.

Machinability characterization

The results of the tangential and feed force variations versus cutting speed for all studied materials are presented in Figure 14 and Figure 15. It can be seen that the machinability of MIP-B, in terms of tangential force, is better than FC-0205PF+MnS alloy and comparable to that of DI 80-55-06 at higher cutting speed (274 m/min). The machinability of MIP-A is comparable to that of FC-0205PF+MnS but inferior to MIP-B and DI 80-55-06. All materials showed better face turning performance at higher speed and at 15° lead angle. This force reduction is due to the increase in the cutting temperature as the cutting speed is increased resulting in a softening action of the work material. Therefore, it is recommended to perform machining at this higher speed in order to increase the tool life. The small reduction in the magnitude of tangential force observed when using the 15° lead angle tool holder could be attributed to the thinning effect imposed on the cut chip. The feed force of MIP-B was comparable to FC-0205PF+MnS but lower than the other materials. It was also found that although the tangential force was lower for DI 80-55-06 compared to FC-0205PF+MnS, it has a lower performance in terms of feed force.

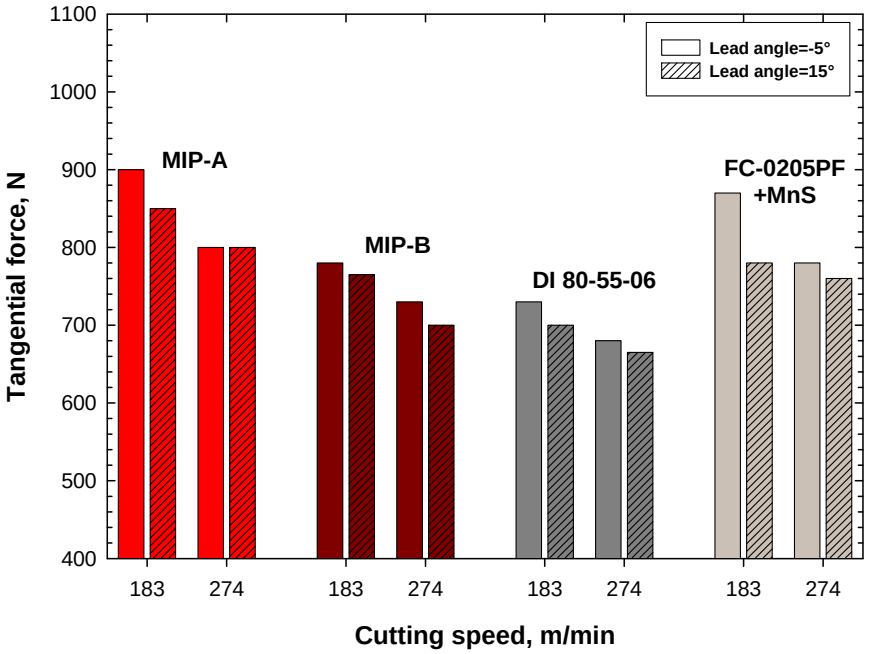

Figure 14. Tangential force versus cutting speed of MIP-A and MIP-B compared to DI 80-55-06 and FC-0205PF+MnS at two different lead angles; semi-roughing operation.

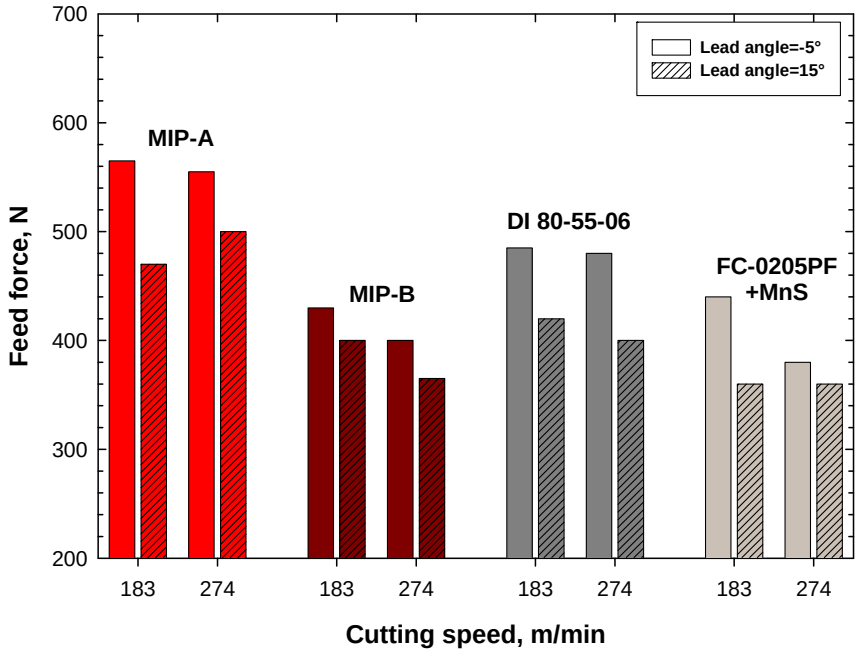

Figure 15. Feed force versus cutting speed of MIP-A and MIP-B compared to DI 80-55-06 and FC-0205PF+MnS at two different lead angles; semi-roughing operation.

For the finishing operation performed at a cutting speed of 137 m/min, the machinability in terms of tangential and feed force was similar for all materials, as depicted in Figure 16 and Figure 17. Although MIP-B had a comparable face turning performance to DI 80-55-06 and FC-0205PF+MnS materials, MIP-A showed a slightly lower performance. For all materials, the tangential force showed a slight increase in magnitude when switching from the -5° to the 15° lead angle as shown in Figure 16 for the finishing

operation. The feed force was similar or lower at 15° lead angle for DI 80-55-06 and FC-0205PF+MnS but slightly higher for MIP materials (Figure 17).

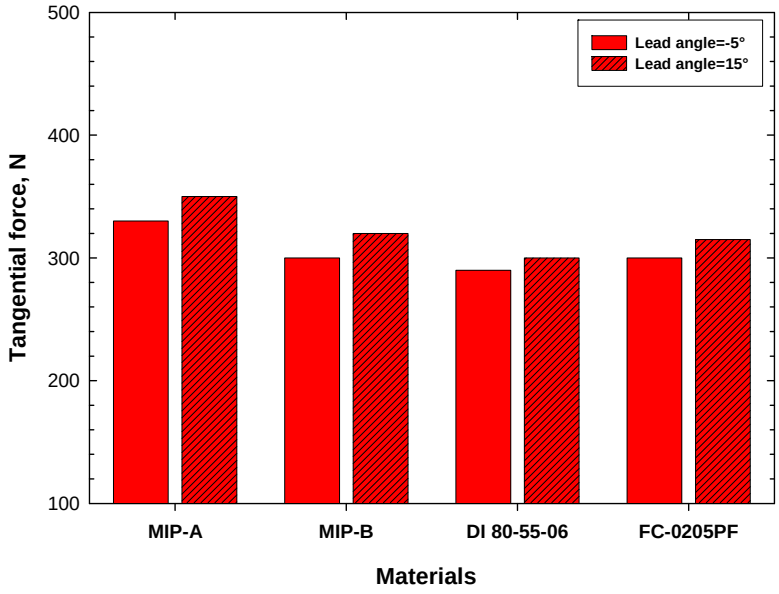

Figure 16. Tangential force of MIP-A and MIP-B compared to DI 80-55-06 and FC-0205PF+MnS at two different lead angles; finishing operation.

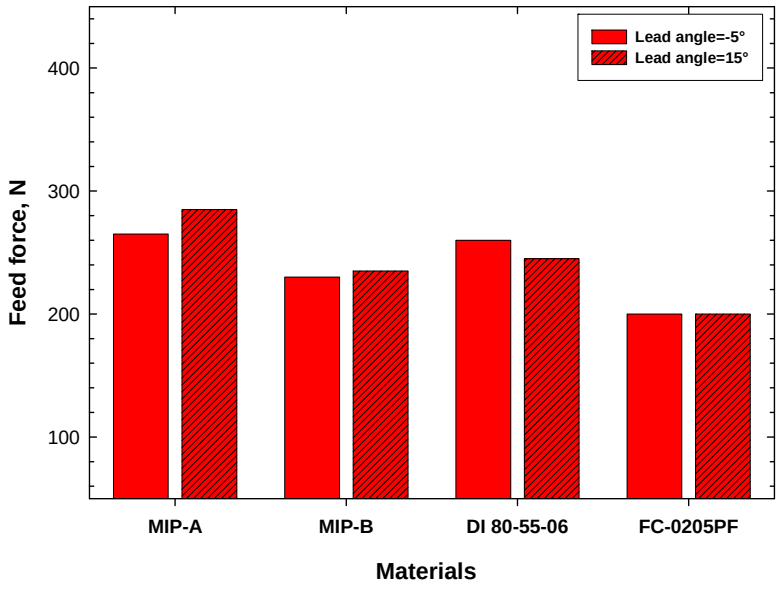

Figure 17. Feed force of MIP-A and MIP-B compared to DI 80-55-06 and FC-0205PF+MnS at two different lead angles; finishing operation.

The microstructures of DI 80-55-06 and FC-0205PF+MnS are shown in Figure 18. Both structures are ferritic-pearlitic and the latter has finer grain size and a larger proportion of ferrite. Although MIP-B indicated a comparable machinability to DI 80-55-06, it possesses superior mechanical properties (Table 6) which could be attributed to its finer microstructure. The mechanical properties of FC-0205PF+MnS[8]

are comparable to that of MIP materials. Meanwhile, the lower machinability of MIP-A can be attributed to its lower content of graphite clusters compared to MIP-B.

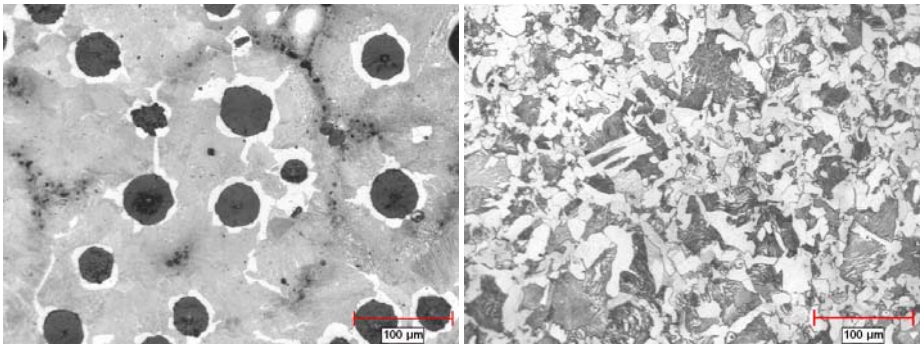

DI 80-55-06 **FC-0205 PF+MnS**

Figure 18. Microstructures of DI 80-55-06 and FC-0205 PF +MnS materials.

Table 6. Tensile properties of the various materials compared.

Materials	Tensile strength, MPa (ksi)	Yield strength, MPa (ksi)	Elongation, %	Hardness, HRC
MIP-A	795 (115)	572 (83)	1.8	29
MIP-B	868 (126)	592 (86)	2.5	28
DI 80-55-06 [7]	700 (102)	470 (68)	8	23
FC-0205 PF+MnS [8]	860 (125)	560 (81)	15	24

CONCLUSIONS

This study carried out with malleable iron powder (MIP) has shown that:

- The shape of the graphite particles in sintered MIP specimens can be modified by addition of 0.2% P (as ferrophosphorus) and makes the sintering possible at lower temperature to achieve a microstructure with a high degree of graphite nodularity and a low "nb flakes/mm² >100 µm".

- Constant values of density and dimensional change can be reached with MIP-A and MIP-B materials when sintered in their sintering temperature windows i.e. 1158 to 1166°C for MIP-A and 1118 to 1124°C for MIP-B.

- When sintered in their sintering temperature windows, tensile properties of MIP-A and MIP-B are little affected by the sintering temperature. However, tensile properties of MIP-B samples were slightly better than those of MIP-A.

- Both materials showed similar hardness values.

- Fatigue strength increased with sintering temperature for both materials due to the higher densities reached. Also, nodular graphite shape in MIP-B resulted in about 20% improvement of axial fatigue strength compared to the flaky graphite shape in MIP-A.

- The machinability tests showed that the cutting forces generated when face turning of MIP-B were slightly lower than powder forged FC-0205+MnS. MIP-B also had comparable or better

machinability than DI 80-55-06. However, MIP-A had a lower turning performance than the other studied materials.

- Increasing the cutting speed from 183 to 274 m/min slightly reduced the cutting forces. Tool life test should be therefore conducted using 274 m/min speed.

REFERENCES

1. German, R.M.; "A Quantitative Theory for Supersolidus Liquid Phase Sintering", Powder Metallurgy, 1991, vol. 34, No. 2, pp 101-107.
2. German, R.M.; "Supersolidus Liquid Phase Sintering Part I; Process Review", The International Journal of Powder Metallurgy, American Powder Metallurgy Institute, Princeton, 1990, vol. 26, pp. 23-34.
3. Shivanath, R., Kucharski, K and Jones, P.; "Press and Sinter Process for High Density Components", US patent 6,346,213.
4. Young, E.; "High Density Supersolidus Liquid Phase Sintering of Steel Powders", M. Sc. Thesis, The University of British Columbia, 2001.
5. Chagnon, F. and Coscia, C.; "Development and Properties of a New Malleable Iron Powder Grade", paper presented at the 2012 International Conference on Powder Metallurgy & Particulate Materials in Nashville (PowderMet 2012).
6. Gagné, M., Filippelli, P. and Trudel, A.; "Iron-Graphite Composite Powders and Sintered Articles Produced Therefrom", US Patent 6,358,298.
7. Jenkins, L.R., and Forrest, R.D., "Ductile Iron", in ASM Handbook, Volume 1, Properties and Selection: Irons, Steels, and High Performance Alloys, Section: Cast Iron, ASM International, 2005.
8. Ilia, E., Tutton, K., and O'Neil, M., "Copper and Carbon on Mechanical Properties of Iron-carbon-Copper Alloys for PM Forging Applications", Proceeding of Euro PM2004, Vienna, Austria, 17-21 October 2004.